JOURNAL OF CHEMICAL INFORMATION AND MODELING

Article

pubs.acs.org/jcim

Conformation Control of Abiotic α-Helical Foldamers

Serge Perato,[†,‡] Jade Fogha,[†,‡] Muriel Sebban,[§] Anne Sophie Voisin-Chiret,[†,‡] Jana Sopkova-de Oliveira Santos,*[,†,‡] Hassan Oulyadi,[§] and Sylvain Rault[†,‡]

[†]Normandie Université, France

[‡]UNICAEN, CERMN (Centre d'Etudes et de Recherche sur le Médicament de Normandie UPRES EA 4258-FR CNRS 3038 INC3M, Bd Becquerel), F-14032 Caen, France

[§]Université de Rouen, COBRA-UMR 6014, Rue Lucien Tesnières, F-76821 Mont-Saint-Aignan, France

Supporting Information

ABSTRACT: With the aim to find new protein−protein inhibitors, a three part methodology was applied to oligophenylpyridines. Theoretical ring twist angle predictions have been validated by X-ray diffraction and molecular dynamics simulations with NMR constraints. Careful choice of substituent and nitrogen positions in oligophenylpyridyl foldamer units opens the way to conformational control of the side chain distribution of this α-helix mimic.

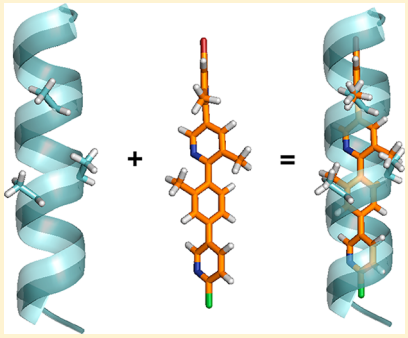

INTRODUCTION

Proteins are the workhorses of the cellular machinery, and the majority of protein functions in living cells involve protein−protein interactions (PPIs).[1] Thus, over time, these interactions have emerged as an important target for biological and pharmaceutical research mainly in neurosciences and cancerology.

An α-helix, as the most abundant secondary structural motif in nature, represents the fundamental recognition element on protein surfaces in many PPIs. Amino acid side chains of a right-handed α-helix are projected outward from the polypeptide backbone that forms the core of this helix. The backbone conformation is stabilized by hydrogen bonds between the amino group of one amino acid and the carbonyl group of an amino acid that is four positions downstream. The side chain of a residue at the ith position therefore lies on the same face as the side chains of the i+3rd (or i+4th) and i+7th etc. residues in the peptide sequence. Commonly, residues situated on the same face ensure the selective and specific recognition in PPIs.[2] Given these features, an α-helix corresponds to an excellent template for the design of potential inhibitors of PPIs.[3]

To date, different approaches have been established to mimic α-helices and then to disrupt α-helix/α-helix interactions. While peptide- and peptidomimetic-based approaches have shown successful applications toward such targets,[4,5] nonpeptide small molecules have advantages in terms of bioavailability and cell permeability. There is therefore considerable interest in developing nonpeptide, small-molecule α-helix mimetics that can disrupt such interactions.[6,7] For instance, Hamilton and co-workers have designed a preorganized nonpeptide α-helix mimetic terphenyl[8,9] as a 3,2′,2″-trisubstituted derivative where methyl groups mimic the ith, i+3rd, and i+7th positions.[10]

From a predictive computational study, Che et al. have proposed that a pyridyl-based scaffold should be more flexible in the α-helix mimicking regions with respect to a phenyl-scaffold and that it should be superior as a helical surface mimetic.[11] Subsequently, Hamilton and co-workers have synthesized terpyridyl scaffolds using sequential Bohlmann-Rahtz heteroannulation reactions.[12] However, due to the difficulty of preparing such compounds as foldamers, many research groups have developed new scaffolds with various (hetero)aromatic rings.[13,14] Among these, our laboratory has described a methodology to design foldamers using pyridyl, thiophenyl and phenyl rings as structural chemical units: the Garlanding concept.[15−20]

Previously, in an in-depth study, we have demonstrated that the oligopyridyl scaffolds could be considered as α-helical mimics.[21] In the present paper, we extend our study to oligophenylpyridyl scaffolds. How will helicity change when a phenyl ring is introduced in the oligopyridyl scaffold? Will these scaffolds be able to mimic the side chain distribution of an α-helix? To answer these questions, our studies were conducted in three steps: first, theoretical simulations were carried out in order to evaluate preferential torsion angles between rings in the phenylpyridyl system. Next, the theoretical predictions were compared with experimental structural data in solid state (X-ray diffraction) and in solution (NMR associated with dynamic

Received: June 25, 2013
Published: September 15, 2013

Table 1. Structural Parameters of Minimum Energy Conformers of Methyl Substituted Phenylpyridine Obtained from PES at the HF/2-31G Level

Group	Compound	Preferential angle between the ring planes[a]	Potential energy barrier [kcal/mol]
A	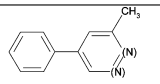 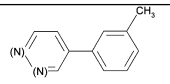 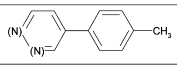 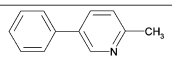	±50° (±35° - ±70°)	3.0 - 3.5
B	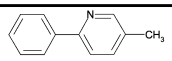 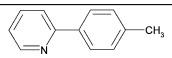 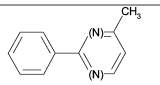 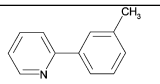	Co-planar (0°- ±35°)	4.5
C	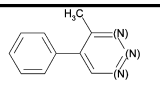 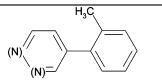	Large minimum from ±70 to ±90 (±55° - ±90°)	10-10.5
D	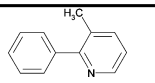	±45° (±30° - ±60°)	3.0
E	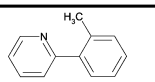	±50° (±35° - ±70°)	3.75

[a]Values in parentheses correspond to a 0.5 kcal/mol limit.

simulations). Finally, we assessed the ability of oligophenylpyridyl substituents to mimic an α-helix side chain distribution.

■ EXPERIMENTAL SECTION

Conformational Analysis. 3D models for all possible phenylpyridines as a function of the pyridyl nitrogen and methyl positions were built using the Discovery Studio software.[22] This corresponds to 32 phenylpyridyl models substituted with one or two methyl groups. The Cartesian coordinates of each model were used as input for the *ab initio* simulation. All *ab initio* calculations reported in the present study were carried out using the Gaussian 03 software.[23] Potential energy scan (PES) studies of all substituted phenylpyridines consisted of a (−180°, +180°) geometry optimization with the specified coordinate freezing and a 5° increment in order to obtain the internal energy barrier to rotation at the HF/6-31G level.

General Procedure for Suzuki−Miyaura Cross-Coupling. Commercial reagents were used as received without further purification. A mixture of pyridylboronic acid or ester (1.25 equiv), 5′-bromo-6-iodo-3′,5-dimethyl-3,2′-bipyridine 1 (1.0 equiv), tetrakis(triphenylphosphine) palladium (5 mol %), and aqueous K_3PO_4 (2.5 equiv) in 1,4-dimethoxyethane was heated to reflux for 20h until the complete consumption of dihalobipyridine 1 (TLC). Crude products were purified by silica gel column chromatography to give 5′-bromo-3′,5-dimethyl-6-(3-methyl-4-pyridin-3-ylphenyl)-3,2′-bipyridine **1**, 5′-bromo-3′,5-dimethyl-6-(2-methyl-4-pyridin-3-ylphenyl)-3,2′-bipyridine **2**, 5′-bromo-3′,5-dimethyl-6−2-methyl-4-(4-chloro-pyridin-3-yl)pheny-3,2′-bipyridine **3**, and 5′-3-methyl-4-(4-chloro-pyridin-3-yl)phenyl-3′,5-dimethyl-6−3-methyl-4-(4-chloro-pyridin-3-yl)phenyl-3,2′-bipyridine **4**, with 71%, 65%, 77%, and 8% yield, respectively.[19]

X-ray Diffraction. Single crystal X-ray analysis was carried out using graphite-monochromatized Mo Kα radiation on a Bruker-Nonius Kappa II diffractometer equipped with a CCD area detector. The crystal structure was solved by direct methods using the SHELX97 package[24] and refined using SHELXL.[25] The refinement was based on F^2 for all reflections, and all non-hydrogen atoms were refined anisotropically. Hydrogen atom positions were determined either via difference Fourier maps and refined with isotropic atomic displacement parameters or were calculated and fixed in ideal geometry, depending on data quality.

NMR Measurements. All NMR experiments were carried out using a Bruker AVIII 600 spectrometer (Bruker, Wissembourg, France) equipped with a 10 A gradient amplifier and a 5 mm CPTXI{^{1}H, ^{13}C,^{15}N} including shielded z-gradients. Solutions with concentrations in the range of 20−30 mg·mL^{-1} in $CDCl_3$, with DMSO-d_6 for phenylpyridine **2**, were

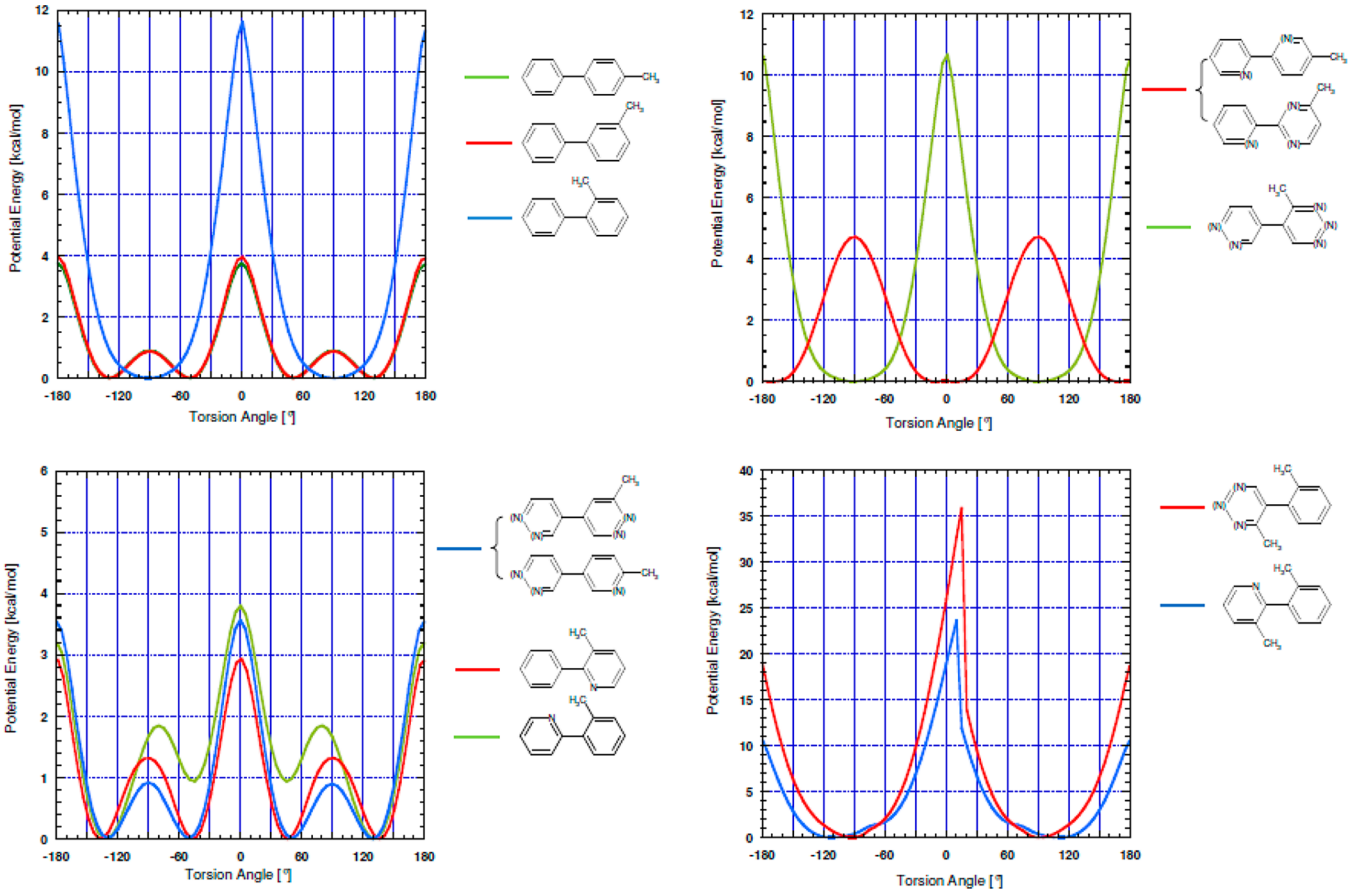

Figure 1. Evolution of potential energy as a function of torsion angle between the rings: (a) biphenyl system substituted by methyl group, (b), (c) phenylpyridyl system with methyl substituent, and (d) phenylpyridyl system with two methyl substituents.

used. Experiments were carried out at 600 MHz for ^{1}H and 150 MHz for ^{13}C. ^{1}H and ^{13}C chemical shifts were referenced according to the $CDCl_3$ solvent signal used as a secondary internal reference (^{1}H, δ = 7.26 ppm; ^{13}C, δ = 77 ppm, with respect to TMS, 0 ppm). The 1D and 2D NMR spectra were obtained at 298 K. Complete assignment of all protons and carbons was carried out using conventional 2D experiments: COSY (^{1}H−^{1}H), NOESY (^{1}H−^{1}H), HSQC (^{1}H−^{13}C), and HMBC (^{1}H−^{13}C). For all 2D spectra, a total of 2048 points in F2 and 512 experiments in F1 were recorded. For the HMBC experiment, an evolution delay of 65 ms was chosen in such a way that correlations involving long-range J coupling around 8 Hz could be observed. The NOESY experiments were performed using mixing times of 1.5 s. Processing and analysis of the NMR spectra was performed with the Topspin 2.1 software from Bruker on a PC workstation.

Molecular Modeling with NMR Constraints. Three dimensional NMR structures of phenylpyridines were refined using the CHARMM program[26] with potential function parameter set 22 from Discovery Studio.[22] The Discovery Studio program was used to derive CHARMM force field parameters for the phenylpyridines applying MMFF partial charges. In the simulations we used only the force field derived by the Discovery Studio without the introduction of supplementary dihedral force field parameters based on our mechanic quantum simulations. To verify the molecular-mechanics force fields obtained, the structures were energy minimized, and their molecular geometry was compared with the X-ray structures. The root-mean-square deviation (RMSD) between the X-ray and the optimized NMR structure was <0.1 Å for all structures. During all CHARMM simulations, NOE (distance) restraints were applied with a force constant of 25 kcal/mol. Starting from the energy minimized X-ray structure, a dynamics simulation of 50 ns was carried out for each derivative at 300 K, with a time step of 1 fs. The dynamics were preceded by a heating (during 6 ps) and equilibration (50 ps) step. During the production phase (10 ns), conformations were saved every 5 ps and energy minimized to a root-mean-square gradient of less than 0.001 kcal/(mol·Å^2). The 10 lowest-energy conformations obtained for each phenylpyridyl compound were used in the subsequent analysis. The selected structures were analyzed and displayed using Discovery Studio.

■ RESULTS AND DISCUSSION

First of all, theoretical simulations have been carried out on simple systems constituted of one pyridyl and one phenyl ring substituted by one or two methyl groups (monosubstituted and bisubstituted systems). In the monosubstituted system, the methyl substituent was placed either on the pyridyl or phenyl ring in different positions. The nitrogen position in the pyridyl ring also varied. In total, 19 models were built, 10 were substituted on the pyridyl and 9 on the phenyl ring. Among the 10 models with methyl substituted on a pyridine, 4 were in the *ortho* position, 4 in the *meta* position, and 2 in the *para* position (relative to the ring junction). In the case of the 9 models substituted on a phenyl ring, for each methyl position, 3 models were built. The behavior of the phenylpyridyl system

substituted on both rings (bisubstituted system) was also evaluated.

For each model the internal potential energy barrier was calculated by *ab initio* simulation as a function of the torsion angle between the two rings. The results for monosubstituted phenylpyridine are summarized in Table 1 and Figure 1. Detailed analysis of the results showed that the 19 monosubstituted models can be divided into 5 groups depending on the preferential twist angle between adjacent pyridyl/phenyl rings and the energy barrier height associated with the pyridyl/phenyl twist.

Among the monosubstituted structures, when the four atoms in the junction vicinity are CH (group A), independently of the methyl substituent position (*para* or *meta*), the steric repulsion between the ortho hydrogens dominates somewhat over symmetric interactions of the π orbital and the ring preferential twist angle is about 50° with a small energy barrier ($\Delta E \sim 3.0$–3.5 kcal/mol). The replacement of one CH group by nitrogen in *ortho* to the junction (group B) reduces the steric repulsion and the π orbital symmetric interaction dominates. The favorite ring orientation becomes indeed coplanar (methyl substituent in *para* or in *meta*), and the energy barrier in this group is somewhat higher with respect to group A ($\Delta E \sim 4.5$ kcal/mol) probably due to weak electrostatic interaction occurring between nitrogen and the CH group situated in front of it.

On the other side, the introduction of the methyl substituent in the *ortho* position to the phenyl/pyridyl junction (the three other atoms in the junction vicinity are CH − group C) leads to more important steric repulsion and therefore to a higher potential energy barrier ($\Delta E \sim 10$–10.5 kcal/mol) with a preferential perpendicular ring position.

Furthermore, in the *ortho* methyl substituted systems, the introduction of the nitrogen in *ortho* to the junction reduces the steric repulsion and increases the symmetric interaction of the π orbitals, as in group B. The preferential ring twist angle becomes indeed about 45° (group D) or 50° (group E). The energy barrier height is close to that of group A ($\Delta E \sim 3$ kcal/mol − group D, $\Delta E \sim 3.75$ kcal/mol − group E).

Finally, as in the oligopyridyl scaffold, the adjacent phenyl/pyridyl rings are balanced by three competing factors: (i) a symmetric interaction between the π orbitals of the aromatic rings, (ii) a steric repulsion between overlapping *ortho* hydrogen atoms and substituents,[11] and (iii) electrostatic interaction due to the presence of nitrogen. The nitrogen has a lone pair, which introduces a negative partial charge in the ring. As a phenyl ring does not contain nitrogen in the phenylpyridyl scaffold, the twist between the adjacent rings is influenced somewhat differently. In the phenylpyridyl system all twisted orientations (groups A, C, D, and E) are analogous to ones in the bipyridyl system, but we cannot reach the strongly constrained coplanar orientation observed in the bipyridyl system. Furthermore, in the bipyridyl systems, the presence of two nitrogens in the vicinity of the junction guided systematically the preferred orientation of these systems with nitrogen positions in *trans* around the junction. In the phenylpyridyl system this situation does not exist: there are never two nitrogens in the vicinity of the junction.

In the case of the bisubstituted models, we observed that the addition of a second substituent in the *meta* or *para* position does not change either the calculated twist angle value or the energy barrier height (data not shown) with the exception of two substituents placed in *ortho* (Table 2, Figure 1). For the *ortho* bisubstituted models, two cases were observed. First, when the nitrogen does not lie in the proximity of the junction, the energy barrier is high ($\Delta E \sim 35$ kcal/mol) and the preferential plane twist angle is about 90°. If the nitrogen is situated in the vicinity of the junction, the energy barrier is smaller ($\Delta E \sim 23$ kcal/mol), and the preferential twist angle is somewhat smaller at about 70°.

Table 2. Structural Parameters of Minimum Energy Conformers of Bisubstituted Ortho Methyl Phenylpyridine Obtained from PES at the HF/2-31G Level

Compound	Preferential angle between the ring planes[a]	Potential Energy Barrier [kcal/mol]
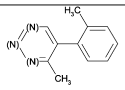	±90° (±75° - ±90°)	35
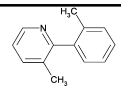	±70° (±50° - ±90°)	23

[a]Values in parentheses correspond to a 0.5 kcal/mol limit.

The analysis of a phenylpyridyl system and an α-helix showed that one aromatic ring with its junction mimics approximately one turn of an α-helix. The axial distance between two successive α-helical turns is about 4.5 Å,[11] and the distance between *ortho* methyl substituents of two adjacent rings is about 5 Å. To mimic a side chain distribution of one face of an α-helix, a twist angle between two consecutive rings close to 40° (angle between i^{th} and i+3rd residue) or 60° (angle between i^{th} and i+4th residue) is appropriate. Our simulations suggested that the monosubstituted phenylpyridyl system is able to introduce a twist angle close to 45°or 50° with a small energy barrier ($\Delta E \sim 3$–3.5 kcal/mol) and therefore flexible enough to reach 40° or 60° without a high energy penalty ($\Delta E_{penalty} \sim 0.2$ kcal/mol). A twist angle of about 70°–90° can be introduced with a higher energy barrier ($\Delta E \sim 10$–10.5 kcal/mol), the energy penalty of this system moving toward 60° is about 0.5 kcal/mol and toward 40° somewhat higher, about 2 kcal/mol. In the bisubstituted system, the preferential angle between the adjacent ring planes is either 70° or 90° as a function of the nitrogen being present in *ortho* to the junction or not. In the first case the energetic penalty of moving to 60° is only minimal ($\Delta E_{penalty} \sim 0.1$ kcal/mol), but the penalty of moving to 40° is about 1.3 kcal/mol. The latter case (nitrogen absence in *ortho* to the junction) permits only to approach the value of 60° ($\Delta E_{penalty} \sim 2$ kcal/mol) and not the value of 40° ($\Delta E_{penalty} \sim 6$ kcal/mol).

The theoretical prediction results using our simple system suggest a possible similitude with the side chain distribution of an α-helix. In order to compare this simple system with a more complex one, experimental structure studies have been carried out. The several phenylpyridines with four or six units were synthesized using the Garlanding method (Figure 2).[19] Suitable crystals for X-ray diffraction study were obtained for four derivatives, and their 3D structures have been determined.

Crystal observation under microscope showed for each derivative only one crystal type (needles) with probably no polymorphisms. The X-ray structures obtained can therefore be considered as representative. For each crystallized compound, the crystal space group contains a symmetric center, and consequently two axial enantiomers are present in each crystal.

The crystal structures of phenylpyridines **1**, **2**, **3**, and **4** show that the rings in the scaffold turn as expected (Figure 3). We

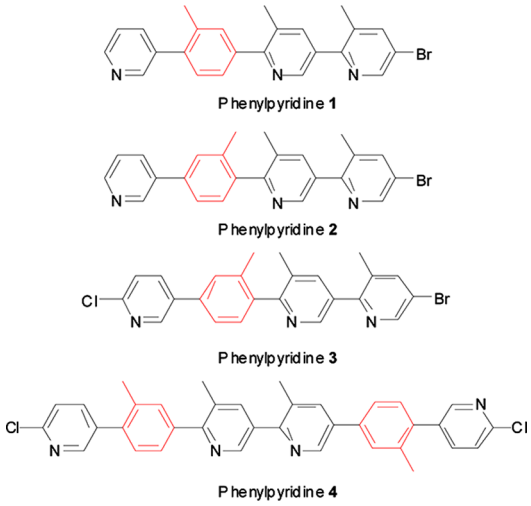

Figure 2. Synthesized phenylpyridines **1**−**4**.

compared first the theoretical prediction of ring twist angles from the corresponding bipyridyl[21] or phenylpyridyl model with the ring twist angles observed in the crystal structures at absolute value level. When a bicycle was substituted in *ortho* and at the same time in *meta* positions, the theoretical prediction associated with *ortho* substitution was used. As we mentioned before, the theoretical simulations showed that the addition of a second substituent in the *meta* or *para* position does not influence the mutual orientation of the rings. Among the four structures solved we observed only one important difference between the predicted and observed value in the case of phenylpyridine **2** (Figure 3). In this experimental structure, the A ring was disordered and two ring conformations were refined. For the first disorder conformation of the A ring, the rings twist angle to B was 20.22°, and for the second disorder conformation it was 11.42°. The predicted favorable twist angle for this junction is between 35 and 70°. However, as the energy barrier about this junction is only 3.5 kcal/mol (Table 1), these deviations introduced a conceivable energetic penalty of about 3 kcal/mol for the twist angle 11.42° and 2 kcal/mol for the twist angle 20.22° (Figure 1). Another fact which is necessary to consider is that the final structure in the crystal is also influenced by intermolecular interactions. Indeed, in the crystal packing weak electrostatic interactions between the pyridine nitrogen and aromatic carbon atom were detected.

In order to characterize 3D structures of our molecules in solution, we carried out a NMR study. In the first step, complete assignment of all protons and carbons was carried out using conventional 2D experiments: COSY (^{1}H−^{1}H), NOESY (^{1}H−^{1}H), HSQC (^{1}H−^{13}C), and HMBC (^{1}H−^{13}C). The proton chemical shifts values and coupling constants of phenylpyridines **1**, **2**, **3**, and **4** are summarized in Table 3 (Full NMR data are available in Supporting Information Table S1). In a second step, we used the NOESY experiment to access the conformations of molecules in solution.[27] Indeed a correlation peak between two protons observed in the 2D spectrum indicates these two nuclei are close through space (strong NOE intensities: distance between protons ≤2.5 Å; medium NOE intensities: distance between protons ≤3.7 Å; weak NOE intensities: distance between protons ≤5.0 Å). An example of a NOESY spectrum is shown in Figures 4 and 5.

In Figure 4, we can observe as expected a spatial proximity between methyl groups and neighboring protons like CH_3B/6B, CH_3C/3C, and CH_3D/3D but also with some protons of the adjacent ring (CH_3C/3B and CH_3D/5C). In the aromatic area (Figure 5) we observed NOE correlations indicating two different spatial proximities: first, intracycle proximity between protons 1A, 2A, and 3A but also proximity of the four protons located on either side of the A-B ring junction. For each phenylpyridine, these observations highlight the nonplanar conformation of the analyzed compounds.

In addition, NOESY allows a quantitative estimation of internuclear distances in small- to intermediate-size molecules.[28] NOE intensities (I) depend on ^{1}H−^{1}H distances as follows: $I = k/r^6$. The constant k is estimated from the integration of a NOE correlation spot between two intracycle protons separated by a distance r, known or determined through X-ray structure and *a priori* independent of molecule conformation. We then decided to perform calculations using several different references whenever possible. By integrating the volumes of correlation spots and using the relation ($I = k/r^6$), we obtained an estimation of the corresponding distances with an error margin of 20 to 25% (due to spin diffusion, other relaxation mechanism, complicated modes of motion, affecting NOEs intensities). The results concerning this study are available in the Supporting Information (Table S2). However, a summary is presented in the following table (Table 4).

As expected, intracycle distances such as CH_3B/6B, CH_3C/3C, and CH_3D/3D estimated by NMR are of the same order of magnitude as the distance deducted from X-ray structures as those corresponding to the A ring. In contrast, intercycle distances like CH_3D/5C, 5A/6B, 3A/2B, and 5A/2B, depending on the conformation in solution, are lower than those observed in solid state. In order to evaluate the influence of the solvent, we performed the same analysis in DMSO-d_6 (see Table S3). Although the chemical shifts are different, the same correlation spots were observed, and their integration leads to the same results as in $CDCl_3$. In view of these results, the difference between the analysis in the solid state and in solution affects only the intercycle distances. These distances are lower than those observed in the solid state, suggesting that the flip is more important in solution.

Molecular dynamic simulations were then carried out with the application of ^{1}H−^{1}H distance constraints determined from the NMR study (NMR constraints). Starting from X-ray structure coordinates, these simulations led to NMR phenylpyridyl 3D structures. For each derivative the ten lowest energy conformers (as shown in Table S4) were retained for subsequent analysis. All ten conformers of **4** were very close, and the rings had turned in the same way. The observed variation of twist angle values was smaller than 1°. For phenylpyridine **3**, the conformers can be divided into two groups which differ from each other only at the A or B ring twist. For phenylpyridines **1** and **2** the ten conformers can be grouped in 3 conformers. For phenylpyridine **2** the differences among the conformers are in the A or/and D ring and for phenylpyridine **1** in the C or/and D ring. The observed differences among NMR conformers of one compound are related to a rotation in the opposite sense of one or two rings. This observation is in agreement with the theoretical predictions that showed that all phenylpyridines can rotate left and right with equal probability.

As in the crystal structure analysis, the NMR structures were compared to the theoretical predictions (Figure 3). The NMR data presented in Figure 3 corresponds to the average of the absolute twist angle values of the ten conformers for each

(i)

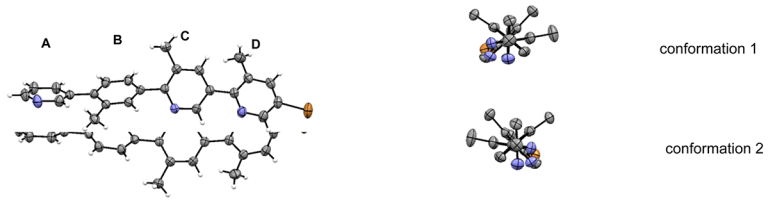

	∠ Ring A-Ring B	∠ Ring B – Ring C	∠ Ring C – Ring D
Prediction	±55° - ±90° (Δ*E*~10kcal/mol)	±30° - ±60° (Δ*E*~3kcal/mol)	±35° - ±70° (Δ*E*~3kcal/mol)
X-ray data			
conformation 1	-52.93	-47.80	-38.18
conformation 2	+52.93	+47.80	+38.18
NMR data	87.9°±0.5	49±2	51°±10

(ii)

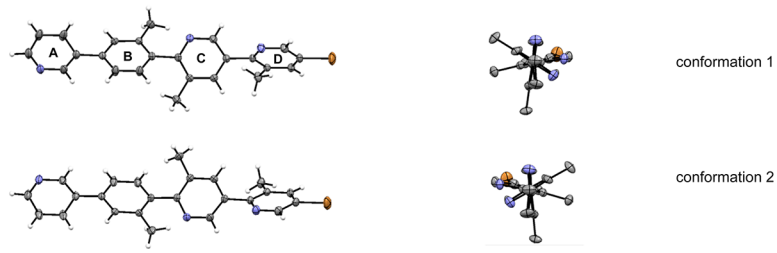

	∠ Ring A- Ring B	∠ Ring B – Ring C	∠ Ring C – Ring D
Prediction	±35° - ±70° (Δ*E*~3kcal/mol)	±50° - ±90° (Δ*E*~23kcal/mol)	±35° - ±70° (Δ*E*~3kcal/mol)
X-ray data			
conformation 1	-11.42° +20.22°	+66.41°	+42.15
conformation 2	+11.42° -20.22°	-66.41°	-42.15
NMR data	63.9°±0.4	56.0°±0.5	43.6°±0.5

(iii)

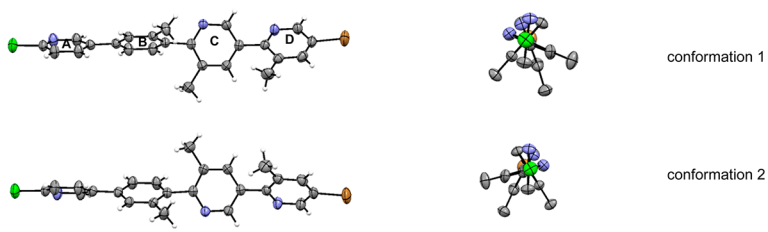

	∠ Ring A- Ring B	∠ Ring B – Ring C	∠ Ring C – Ring D
Prediction	±35° - ±70° (Δ*E*~3kcal/mol)	±50° - ±90° (Δ*E*~23kcal/mol)	±35° - ±70° (Δ*E*~3kcal/mol)
X-ray data			
conformation 1	-34.40°	-72.30°	-45.55
conformation 2	+34.40°	+72.30°	+45.55
NMR data	79°±1	61.79°±0.03	64.14°±0.02

Figure 3. continued

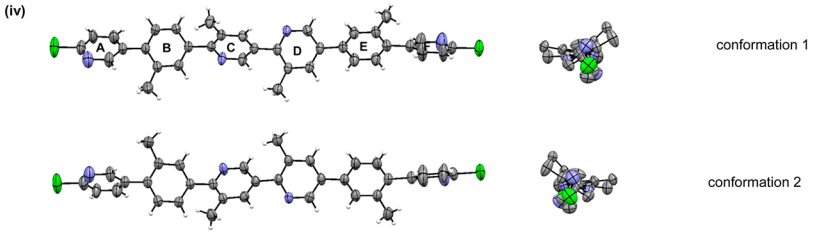

	∠ Ring A-Ring B	∠ Ring B – Ring C	∠ Ring C – Ring D	∠ Ring D – Ring E	∠ Ring E – Ring F
Prediction	±55° - ±90° (Δ*E*~10kcal/mol)	±30° - ±60° (Δ*E*~3kcal/mol)	±35° - ±70° (Δ*E*~3kcal/mol)	±35° - ±70° (Δ*E*~3kcal/mol)	±55° - ±90° (Δ*E*~10kcal/mol)
X-ray data					
conf 1	+60.00	+42.18	-47.86	+40.09	+63.45
conf 2	-60.00	-42.18	+47.86	-40.09	-63.45
NMR data	52.14±0.01°	56.20±0.07°	53.47±0.07°	38.74±0.02°	52.75±0.03°

Figure 3. ORTEP view (2 mutually perpendicular views) of the two conformers from crystal structures and the twist angle values of phenypyridine **1** (i), **2** (ii), **3** (iii), and **4** (iv). Displacement ellipsoids are drawn at the 50% probability level, and H atoms are shown as small spheres of arbitrary radii.

Table 3. ^{1}H NMR Data ($CDCl_3$)

		1	2	3	4
cycle A	H1	8.61	-	-	8.65−8.62
	H2	7.37	7.42	7.41	7.42
	H3	7.69	7.68	7.88	7.97−7.95
	H4	-	-	-	-
	H5	8.65	8.43	8.65	8.93
	H6	-	-	-	-
cycle B	H1	-	-	-	-
	H2	2.34	2.35	7.46	7.55−7.52
	H3	7.54	7.55	7.33	7.38
	H4	-	-	-	-
	H5	7.47	7.48	2.22	2.26
	H6	7.31	7.30	7.49	7.55−7.52
cycle C	H1	-	-	-	-
	H2	2.49	2.49	2.23	2.28
	H3	7.80	7.81	7.81	7.97−7.95
	H4	-	-	-	-
	H5	8.70	8.70	8.68	8.80
	H6	-	-	-	-
cycle D	H1	-	-	-	-
	H2	2.44	2.46	2.46	2.57
	H3	7.79	7.81	7.81	7.68
	H4	-	-	-	-
	H5	8.62	8.64	8.64	8.65−8.62
	H6	-	-	-	-
cycle E	H1	-	-	-	-
	H2	-	-	-	7.55−7.52
	H3	-	-	-	7.55−7.52
	H4	-	-	-	-
	H5	-	-	-	2.46
	H6	-	-	-	7.57
cycle F	H1	-	-	-	8.65−8.62
	H2	-	-	-	7.42
	H3	-	-	-	7.97−7.95
	H4	-	-	-	-
	H5	-	-	-	8.93
	H6	-	-	-	-

compound. An overview of these results indicates that the 3D NMR structures fall into predicted twist angle interval with three exceptions: in compound **3**, the A Ring - B Ring (RA-RB) twist angle; in compound **4** the RA-RB and RE-RF twist angles are slightly out of the predicted value interval. However, the deviations are small, about 8° for RA-RB in **3**, and about 2° for RA-RB and RE-RF in phenylpyridine **4**. These deviations introduce only small energy penalties ($\Delta E_{penalty} \sim 1$ kcal/mol in **3** and $\Delta E_{penalty} \sim 1.5$ kcal/mol for both angles in phenylpyridine **4**) (Figure 1). These experimental results fully confirmed that the theoretical predictions from the biphenylpyridyl models are reproduced in longer models in solid state (crystal structures) as well as in solution (NMR structures).

To validate the hypothesis that the substituents on the oligophenylpyridyl scaffolds will be found in side chain positions of an α-helix, our four molecules (NMR and X-ray structures) were superimposed with an ideal polyalanyl α-helix (Figure 6). The oligophenylpyridyl scaffolds were aligned along the helix axis, and we observed that substituents were projected well at the different α-helix positions. In conclusion, the substituent positions of all studied compounds coincided well with the positions of certain α-helical side chains.

We have demonstrated that the phenylpyridyl system can present a different twist angle between two consecutive rings as a function of substituent and/or nitrogen position. Therefore, depending on the helix side chain(s) which we want to mimic, the sequence of building blocks, substituent position, and nitrogen position in a phenylpyridyl unit should be carefully chosen. For example, if we want to mimic a side chain at i^{th} and i+4th positions, a twist angle close to 40° must be introduced between two consecutive rings. For this, different phenylpyridyl building blocks can be used. Either one ring can be substituted in *ortho* and the other in *meta* of the junction or both rings can be substituted in *meta* of the junction. In the first case if we want to introduce a twist angle close to 40° without a high energy penalty, the nitrogen atom must be situated in *ortho* of the junction. In the second case all possible nitrogen positions should allow the desired twist angle close to 40° without a high energy penalty.

■ CONCLUSION

This study has demonstrated that the oligophenylpyridyl scaffold can successfully mimic different α-helical twists and

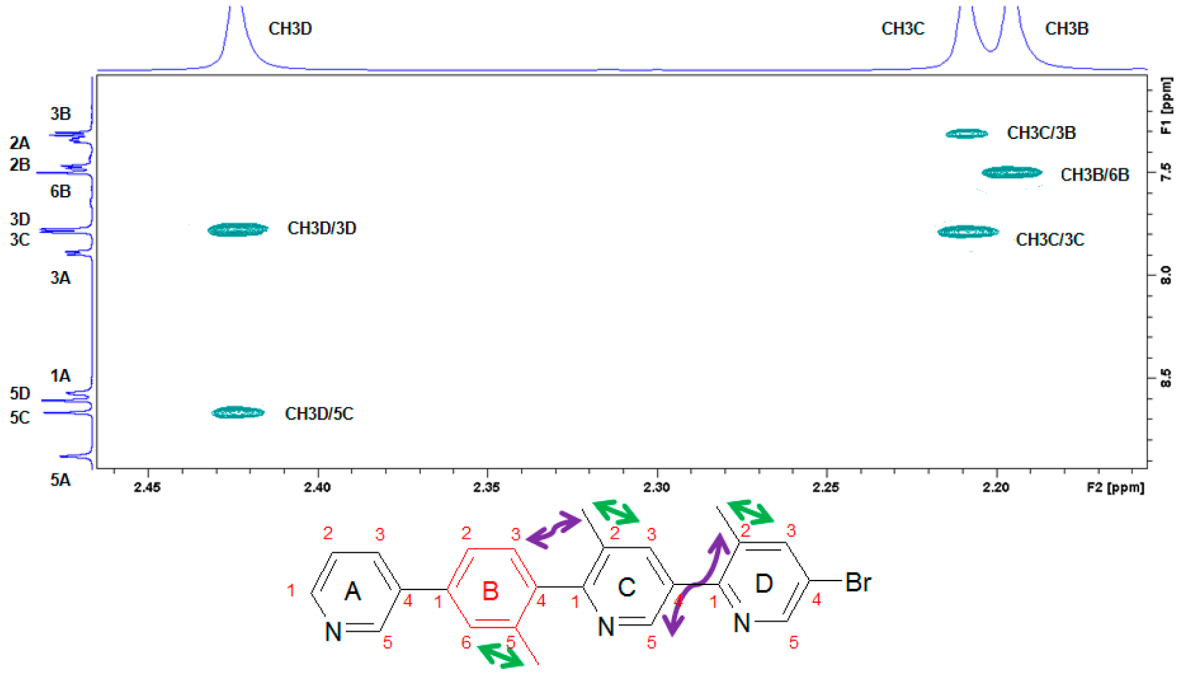

Figure 4. NOESY spectrum of phenylpyridine **2**.

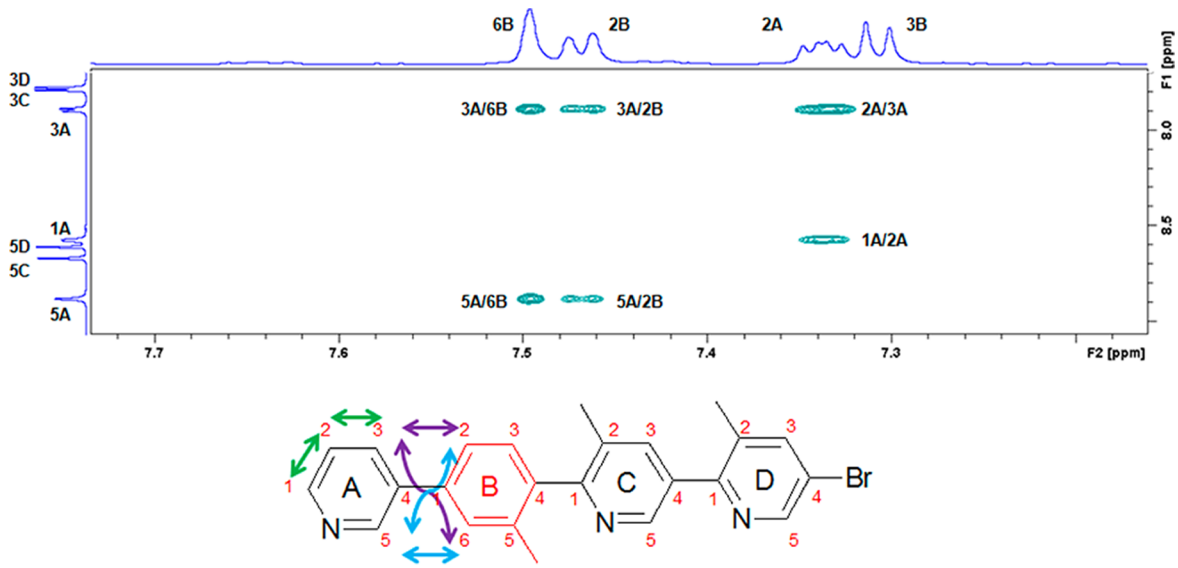

Figure 5. NOESY spectrum of phenylpyridine **2**.

Table 4. Estimated Distances from NMR Spectra and from the X-ray Structure of Phenylpyridine 2

NOE	X-ray distances (Å)	NOE estimated distances (Å)
$CH_3D/3D$	2.854	2.6 ± 0.5
$CH_3D/5C$	4.897	2.9 ± 0.5
$CH_3C/3C$	2.864	2.7 ± 0.5
$CH_3C/3B$	3.171	3.2 ± 0.6
$CH_3B/6B$	2.841	2.6 ± 0.5
2A/3A	2.337	2.2 ± 0.4
1A/2A	2.247	2.4 ± 0.5
3A/6B	2.128	2.5 ± 0.5
5A/6B	4.421	2.5 ± 0.5
3A/2B	4.543	2.5 ± 0.5
5A/2B	2.034	2.6 ± 0.5

therefore mimic different distributions of helical side chains. To achieve this, a careful choice of building block, substituent, and nitrogen positions must be made. Our results show that biphenylpyridyl models predict well the twist angles between two adjacent rings observed experimentally (NMR and X-ray studies) even in longer oligophenylpyridyl scaffolds. The phenylpyridyl scaffolds are able to mimic the α-helical side chains in the same way as the oligopyridyl scaffold evaluated previously in our laboratory[21] and thus belong to a category of abiotic foldamers. The next stage of this work is to introduce various lateral chains on the scaffold in order to interact with protein surfaces. The presence of a phenyl ring will allow considering numerous reactions such as C−H activation which is largely described on pyridine or phenylpyridine in order in to functionalize such oligomers.[29,30]

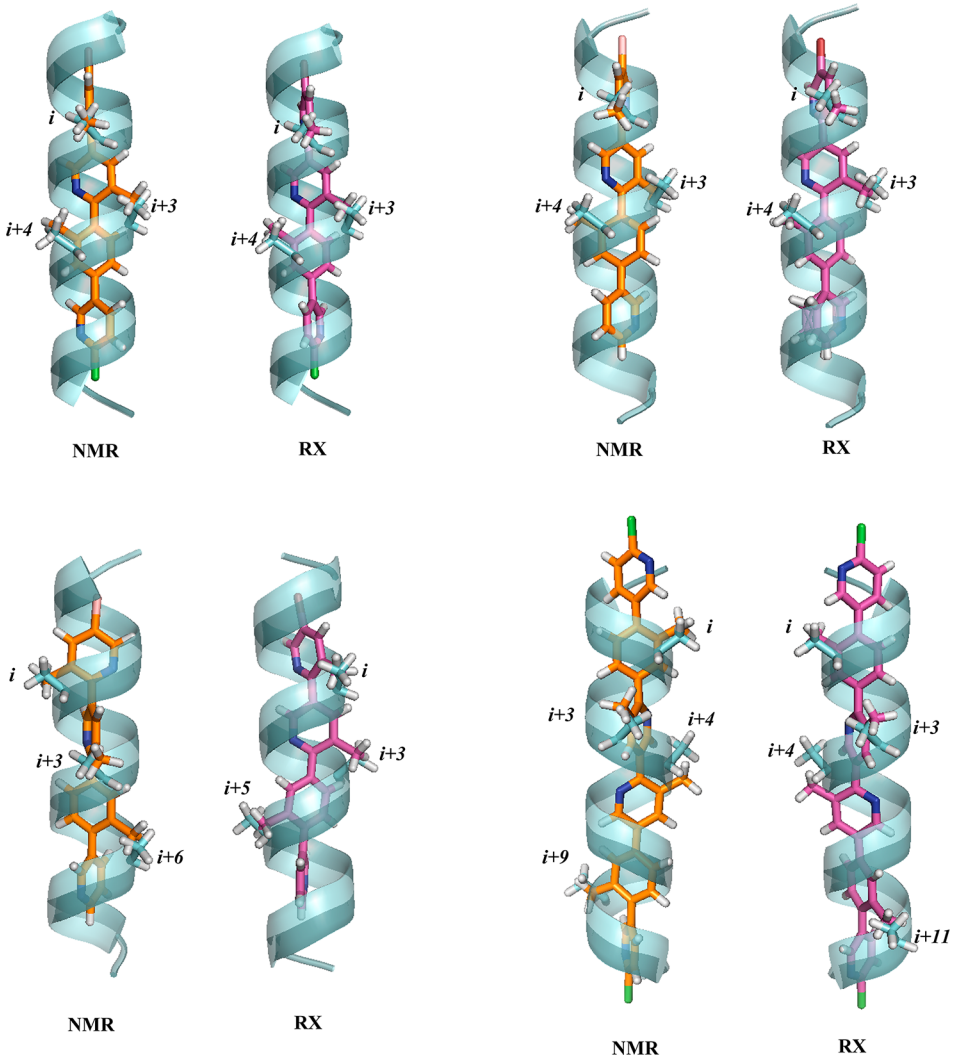

Figure 6. Superposition of a polyalanyl α-helix (in blue) and NMR structure (in orange) or X-ray structure (in purple) of phenylpyridines **1**, **2**, **3**, and **4**.

■ ASSOCIATED CONTENT

Supporting Information

Proton chemical shifts values and coupling constants of phenylpyridines, estimated distances from NMR spectra and from X-ray structure of phenylpyridines, twist angle values of the ten lowest energy conformations of phenylpyridine. This material is available free of charge via the Internet at http://pubs.acs.org.

■ AUTHOR INFORMATION

Corresponding Author

*Fax: +33.(0)2.31.56.68.03. E-mail: jana.sopkova@unicaen.fr. Homepage: http://www.cermn.unicaen.fr/. Corresponding author address: Normandie Univ, France; UNICAEN, CERMN (Centre d'Etudes et de Recherche sur le Médicament de Normandie UPRES EA 4258-FR CNRS 3038 INC3M, Bd Becquerel), F-14032 Caen, France.

Notes

The authors declare no competing financial interest.

■ ACKNOWLEDGMENTS

The authors gratefully acknowledge financial support from the 'CRUNCHOrga' (Centre de Recherche Universitaire Normand de Chimie Organique), ERDF funding (ISCE-Chem & INTERREG IVa program), the 'Région Basse-Normandie' and the CRIHAN (Centre de Ressources Informatiques de Haute Normandie), as well as the European Community (FEDER) for the molecular modelling software.

■ REFERENCES

(1) Keskin, O.; Gursoy, A.; Ma, B.; Nussinov, R. Principles of protein−protein interactions: What are the preferred ways for proteins to interact? *Chem. Rev.* **2008**, *108*, 1225−1244.

(2) Edwards, T. A.; Wilson, A. J. Helix-mediated protein-protein interactions as targets for intervention using foldamers. *Amino Acids* **2011**, *41*, 743−754.

(3) Bullock, B. N.; Jochim, A. L.; Arora, P. S. Assessing helical protein interfaces for inhibitor design. *J. Am. Chem. Soc.* **2001**, *133*, 14220−14223.

(4) Pilsl, L. K. A.; Reiser, O. α/β-Peptide foldamers: State of the art. *Amino Acids* **2011**, *41*, 709−718.

(5) Claudon, P.; Violette, A.; Lamour, K.; Decossas, M.; Fournel, S.; Heurtault, B.; Godet, J.; Mély, Y.; Jamart-Grégoire, B.; Averlant-Petit, M.-C.; Briand, J. P.; Duportail, G.; Monteil, H.; Guichard, G. Consequences of isostructural main-chain modifications for the design of antimicrobial foldamers: Helical mimics of host-defense peptides based on a heterogeneous amide/urea backbone. *Angew. Chem., Int. Ed.* **2010**, *49*, 333−336.

(6) Hecht, S.; Huc, I. Foldamers: Structure, properties and applications; Hecht, S., Huc, I., Eds.; Wiley-VCH: Weinheim, 2007.
(7) Zhang, D. W.; Zhao, X.; Hou, J. L.; Li, Z. T. Aromatic amide foldamers: structures, properties, and functions. *Chem. Rev.* **2012**, *112*, 5271−5316.
(8) Yin, H.; Hamilton, A. D. Strategies for targeting protein-protein interactions with synthetic agents. *Angew. Chem., Int. Ed.* **2005**, *44*, 4130−4163.
(9) Saraogi, I.; Hamilton, A. D. α-Helix mimetics as inhibitors of protein-protein interactions. *Biochem. Soc. Trans.* **2008**, *36*, 1414−1417.
(10) Orner, B. P.; Ernst, J. T.; Hamilton, A. D. Toward proteomimetics: Terphenyl derivatives as structural and functional mimics of extended regions of an α-helix. *J. Am. Chem. Soc.* **2001**, *123*, 5382−5383.
(11) Che, Y.; Brooks, B. R.; Marshall, G. R. Development of small molecules designed to modulate protein-protein interactions. *J. Comput.-Aided. Mol. Des.* **2006**, *20*, 109−130.
(12) Davis, J. M.; Truong, A.; Hamilton, A. D. Synthesis of a 2,3′;6′,3″-terpyridine scaffold as an α-helix mimetic. *Org. Lett.* **2005**, *24*, 5405−5408.
(13) Biros, S. M.; Moisan, L.; Mann, E.; Carella, A.; Zhai, D.; Reed, J. C.; Rebek, J. Heterocyclic alpha-helix mimetics for targeting protein-protein interactions. *Bioorg. Med. Chem. Lett.* **2007**, *17*, 4641−4645.
(14) Anderson, L.; Zhou, M.; Sharma, V.; McLaughlin, J. M.; Santiago, D. N.; Fronczek, F. R.; Guida, W. C.; McLaughlin, M. L. Facile iterative synthesis of 2,5-terpyrimidinylenes as nonpeptidic alpha-helical mimics. *J. Org. Chem.* **2010**, *75*, 4288−4291.
(15) Voisin, A.-S.; Bouillon, A.; Burzicki, G.; Célant, M.; Legay, R.; El-Kashef, H.; Rault, S. A general synthesis of halo-oligopyridines. The Garlanding concept. *Tetrahedron* **2009**, *65*, 607−612.
(16) Burzicki, G.; Voisin-Chiret, A.-S.; Sopkovà-de Oliveira Santos, J.; Rault, S. Synthesis of dihalo bi- and terpyridines by regioselective Suzuki-Miyaura cross-coupling reactions. *Tetrahedron* **2009**, *65*, 5413−5417.
(17) Burzicki, G.; Voisin-Chiret, A.-S.; Sopkovà-de Oliveira Santos, J.; Rault, S. Synthesis of new [2,3′:6′,3″]terpyridines using iterative cross-coupling reactions. *Synthesis* **2010**, *16*, 2804−2810.
(18) Voisin-Chiret, A.-S.; Muraglia, M.; Burzicki, G.; Perato, S.; Corbo, F.; Sopková-de Oliveira Santos, J.; Franchini, C.; Rault, S. Synthesis of new phenylpyridyl scaffolds using the Garlanding approach. *Tetrahedron* **2010**, *66*, 8000−8005.
(19) Perato, S.; Voisin-Chiret, A.-S.; Sopková-de Oliveira Santos, J.; Sebban, M.; Legay, R.; Oulyadi, H.; Rault, S. Synthesis of new linear poly(phenylpyridyl) chains. *Tetrahedron* **2012**, *68*, 1910−1917.
(20) De Giorgi, M.; Voisin-Chiret, A.-S.; Sopková-de Oliveira Santos, J.; Corbo, F.; Franchini, C.; Rault, S. Design and synthesis of thienylpyridyl garlands as non-peptidic alpha helix mimetics and potential protein-protein interactions disruptors. *Tetrahedron* **2011**, *67*, 6145−6154.
(21) Sopková-de Oliveira Santos, J.; Voisin-Chiret, A.-S.; Burzicki, G.; Sebaoun, L.; Sebban, M.; Lohier, J.-F.; Legay, R.; Oulyadi, H.; Bureau, R.; Rault, S. Structural characterizations of oligopyridyl foldamers, α-helix mimetics. *J. Chem. Inf. Model.* **2012**, *52*, 429−439.
(22) Discovery Studio, version 3.0; 2005; Accelrys Software Inc.: San Diego, CA. http://www.accelrys.com (accessed Sept 24, 2013).
(23) Frisch, M. J.; Trucks, G. W.; Schlegel, H. B.; Scuseria, G. E.; Robb, M. A.; Cheeseman, J. R.; Zakrzewski, V. G.; Montgomery, J. A., Jr.; Stratmann, R. E.; Burant, J. C.; Dapprich, S.; Millam, J. M.; Daniels, A. D.; Kudin, K. N.; Strain, M. C.; Farkas, O.; Tomasi, J.; Barone, V.; Cossi, M.; Cammi, R.; Mennucci, B.; Pomelli, C.; Adamo, C.; Clifford, S.; Ochterski, J.; Petersson, G. A.; Ayala, P. Y.; Cui, Q.; Morokuma, K.; Salvador, P.; Dannenberg, J. J.; Malick, D. K.; Rabuck, A. D.; Raghavachari, K.; Foresman, J. B.; Cioslowski, J.; Ortiz, J. V.; Baboul, A. G.; Stefanov, B. B.; Liu, G.; Liashenko, A.; Piskorz, P.; Komaromi, I.; Gomperts, R.; Martin, R. L.; Fox, D. J.; Keith, T.; Al-Laham, M. A.; Peng, C. Y.; Nanayakkara, A.; Challacombe, M.; Gill, P. M. W.; Johnson, B.; Chen, W.; Wong, M. W.; Andres, J. L.; Gonzalez, C.; Head-Gordon, M.; Replogle, E. S.; Pople, J. A. *Gaussian 03, Revision A.1*; Gaussian Inc.: Pittsburgh, PA, 2003.
(24) Sheldrick, G. M. Phase annealing in SHELX-90: Direct methods for larger structures. *Acta Crystallogr.* **1990**, *A46*, 467−473.
(25) Sheldrick, G. M. A short history of SHELX. *Acta Crystallogr.* **2008**, *A64*, 112−122.
(26) Brooks, B. R.; Bruccoleri, R. E.; Olafson, B. D.; States, D. J.; Swaminathan, S.; Karplus, M. CHARMM: A program for macromolecular energy, minimization, and dynamics calculations. *J. Comput. Chem.* **1983**, *4*, 187−217.
(27) Neuhaus, D.; Williamson, M. P. The Nuclear Overhauser Effect in Structural and Conformational Analysis, 2nd ed.; John Wiley & Sons, Inc.: New York, 2000.
(28) Jones, C. R.; Butts, C. P.; Harvey, J. N. Accuracy in determining interproton distances using Nuclear Overhauser Effect data from a flexible molecule. *Beilstein J. Org. Chem.* **2011**, *7*, 145−150.
(29) Nakao, Y. Transition-metal-catalyzed C−H functionalization for the synthesis of substituted pyridines. *Synthesis* **2011**, *20*, 3209−3219.
(30) Lyons, T. W.; Sanford, M. S. Palladium-catalyzed ligand-directed C-H functionalization reactions. *Chem. Rev.* **2010**, *110*, 11471169.